Scalable GaInP/GaAs HBT Large-Signal Model

Matthias Rudolph, *Member, IEEE*, Ralf Doerner, *Member, IEEE*, Klaus Beilenhoff, *Member, IEEE*, and Peter Heymann, *Associate Member, IEEE*

***Abstract*—A scalable large-signal model for heterojunction bipolar transistors (HBTs) is presented in this paper. It allows exact modeling of all transistor parameters from single-finger elementary cells to multifinger power devices. The scaling rules are given in detail. The model includes a new collector description, which accounts for modulation of base–collector capacitance $C_{\rm jc}$, as well as for base and collector transit times due to temperature effects and high-current injection. The model is verified by comparison with measurements of GaInP/GaAs HBTs.**

***Index Terms*—Equivalent circuits, heterojunction bipolar transistors, semiconductor device modeling, semiconductor device thermal factors.**

I. Introduction

HETEROJUNCTION bipolar-transistors (HBTs) are favorite devices for power applications in mobile communication systems. This is due to their linearity and ability to operate at high power densities with low collector voltages.

In HBTs, the base is highly doped to reduce sheet resistance, while the collector doping is low in order to minimize base–collector capacitance $C_{\rm jc}$ and to increase breakdown voltage. Therefore, high-current injection first occurs in the collector region. This leads to modulation of the base–collector space charge region and, hence, changes $C_{\rm jc}$ and collector transit time τ_C. Finally, high-current injection causes base push out and an excess base transit time τ_{CIB}. Since the base is very thin, in order to minimize base transit times τ_B, the contribution of the voltage and current dependent τ_C to the total transit time τ_f cannot be neglected.

Various analytical models of τ_{CIB} in Si– and Ge-based bipolar junction transistors (BJTs) have been presented following the initial work of Kirk [1], [2]. Also, different analytical models and numerical simulations for modulation of $C_{\rm jc}$ have been published [3], [4]. These models provide a physical understanding of the effects in the collector.

In GaAs-based HBTs, however, the nonlinear field dependence of the electron velocity and self-heating of the device prevents analytical calculation of $C_{\rm jc}$ and τ_f. Therefore, an empirical description has to be developed, as in [5]. In this investigation, for the first time to the author's knowledge, experimental data is given, which shows the bias and temperature dependence of transit times and $C_{\rm jc}$. The small-signal equivalent-circuit elements are obtained by a method previously published by the authors [6], which allows to distinguish between intrinsic and extrinsic base–collector junction capacitance. An empirical description is developed and implemented into a large-signal model.

A scalable nonlinear model is required for several purposes. From a foundry point-of-view, one requires insight into the large-signal behavior to develop new transistors, and to have small-sized sample devices in order to monitor the process parameters. The designer of monolithic microwave integrated circuits (MMICs), on the other hand, demands for simulation tools to optimize the HBT performance as a function of HBT size for a specific task. Thus, scaling is a central task for HBT modeling when proceeding from "simple" small periphery devices to large high-power transistors.

In the literature thus far, the power performance of a large-scale HBT was predicted from the known electrothermal behavior of its elementary sub-cells and their thermal interaction [7], [8]. The aim was to account for the mutual heating of the emitter fingers in a multifinger device. In other papers, scaling of the small-signal equivalent-circuit elements was investigated [9], [10].

In this paper, a new scaled large-signal model is presented. It is verified for the HBT process type with thermal shunt technology, available at the Ferdinand–Braun–Institut für Höchstfrequenztechnik, Berlin, Germany [11]. All emitters of multifinger transistors are connected with a thick air bridge, which equalizes their temperature in order to prevent thermal runaway. It has been observed that the different HBTs under investigation can be described by the same equivalent circuit. The scaled model is, therefore, obtained by defining the model parameters as a function of HBT geometry. No additional information on thermal or electrical interaction between the emitter fingers is necessary. The new model predicts the electrical behavior of HBTs of different geometry than that device the parameters have been extracted from.

The scaling range extends from a single-finger HBT with an emitter area of $3 \times 30\ \mu\text{m}^2$ to a ten-finger power cell with the tenfold emitter area capable of 30-dBm output power at 2 GHz. As an example, the model parameters are extracted from a single-finger elementary cell and scaled up to ten-finger power cells. Only the thermal resistance $R_{\rm th}$ has been determined for the different types individually.

II. Basic Model

The equivalent circuit is shown in Fig. 1. The extrinsic elements describing the contacts and coplanar test environment are bias independent and, therefore, not shown here. Besides the

Manuscript received March 30, 2000; revised September 15, 2000.

M. Rudolph, R. Doerner, and P. Heymann are with the Microwave Department, Ferdinand–Braun–Institut für Höchstfrequenztechnik, D-12489 Berlin, Germany (e-mail: rudolph@fbh-berlin.de).

K. Beilenhoff was with the Institut für Hochfrequenztechnik, Technische Universität Darmstadt, D-64283 Darmstadt, Germany. He is now with Daimler-Chrysler AG, Stuttgart, Germany.

Publisher Item Identifier S 0018-9480(00)10731-8.

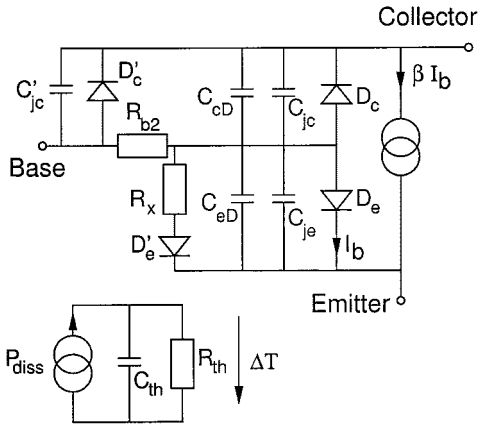

Fig. 1. Large-signal model topology including thermal equivalent circuit.

new description for $C_{\rm jc}$ and τ, the following elements, which depend both on bias and transistor size, are added to the common model.

- A base–collector diode D_c', a capacitance $C_{\rm jc}'$, and an intrinsic base resistance R_{b2} account for the mesa structure of the device.
- A diode D_e' with series resistor R_x models the nonideal base–emitter current due to recombination at the heterojunction. This describes the different ideality factors of base and collector current [12].
- To determine the junction temperature, the well-known thermal equivalent circuit is applied.

The temperature dependence of the base–emitter diodes is modeled using the formula

$$I = I_{s\infty} e^{-V_g/V_{\rm th}} \left(e^{V/(nV_{\rm th})} - 1 \right) \tag{1}$$

with the maximum saturation current $I_{s\infty}$ for $T \to \infty$, an activation energy $E_g = V_g/q$, the thermal voltage $V_{\rm th}$, and the ideality factor n. The temperature dependence of the collector diodes D_c' and D_c is neglected and the temperature-independent formula

$$I = I_s \left(e^{V/(nV_{\rm th})} - 1 \right) \tag{2}$$

applies. Current gain β decreases linearly with temperature.

III. Collector Model

To understand what happens in the collector in the high-current regime, it is useful to define an effective collector doping level

$$N_{C,\,\rm eff} = N_C - \frac{J_C}{qv} \tag{3}$$

with the electron velocity v, the collector current density J_C, the collector doping density N_C, and the electron charge q. This means that the electrons of the collector current compensate the charge of the donors, and the resulting charge is understood as an effective collector doping. Using (3), one can distinguish the following three conditions dependent on the current density J_C:

1) very low current range, with $N_C \gg J_C/(qv)$ and $N_{C,\,\rm eff} \approx N_C$;
2) range of moderate currents, where $N_C > J_C/(qv)$, but of comparable magnitude;
3) high-injection range, with $N_C < J_C/(qv)$.

It is important to note that at $J_C = N_C qv$, the quantity $N_{C,\,\rm eff}$ changes from n- to p doping. Consequently, the p-n-junction shifts from the base–collector interface to the collector–subcollector interface. If the collector is not fully depleted, a neutral region is formed in the collector region at the base–collector junction, which is called current-induced base and leads to an excess base transit time τ_{CIB}. This effect is known as base push out or Kirk effect. The current that determines the onset of base push out is expected to increase with collector-base voltage ($V_{\rm cb}$) since it is determined by the width of the space–charge region. In power HBTs, however, the opposite behavior can be observed for the transit frequency f_t.

From this simple model, it can be expected that modulation of base–collector space–charge region and, hence, $C_{\rm jc}$ and τ_C, has to be considered starting from the range of moderate currents, even below the current density that determines the onset of base push out. $C_{\rm jc}$ and τ_C will depend on collector current as well as on base–collector voltage ($V_{\rm bc}$).

The model presented in this paper is based on empirical formulas since the nonlinear field dependence of electron velocity in the GaAs collector prevents a compact analytical solution of (3) suitable for large-signal modeling. The new description is developed considering small-signal equivalent-circuit elements extracted at various bias points and different ambient temperatures, in order to separate temperature and bias-dependent effects.

A. Capacitances

It is found from measurements that the base–collector capacitances $C_{\rm jc}$ and $C_{\rm jc}'$ are independent of temperature, but depend only on base–collector voltage $V_{\rm bc}$ and collector current-density J_c, as expected from physics. Comparison of total base–collector capacitance $C_{\rm jc} + C_{\rm jc}'$ and intrinsic capacitance $C_{\rm jc}$ [see Fig. 2 (a) and (b)] demonstrates that $C_{\rm jc}$ dominates the total capacitance in the high-injection range. At moderate currents, the large value of $C_{\rm jc}'$ shadows the contribution of $C_{\rm jc}$. Therefore, one has to extract $C_{\rm jc}$ accurately.

At moderate currents, up to $J_c \approx 30$ kA/cm^2, where the collector current lowers the effective doping, $C_{\rm jc}$ decreases accordingly. It can be modeled by the following empirical formula:

$$C_{\rm jc}\,|_{{\rm mod.}J_c} = \begin{cases} C_{jc0} \cdot \left(1 - \dfrac{J_c}{J_0}\right)^m \left(\dfrac{1}{1 - \dfrac{V_{\rm bc}}{\phi_{\rm bc}}}\right)^n, \\ \qquad \text{for } C_{\rm jc} > C_{jc\,\min} \\ C_{jc\,\min}, \qquad \text{else} \end{cases} \tag{4}$$

with $J_0 = J_{0b} - J_{0a} V_{\rm bc}$, where J_{0b}, J_{0a}, and m are fitting parameters. For the HBTs under investigation, $m = 1$, i.e., $C_{\rm jc}$, decreases linearly with current. This has also been observed by other authors [13]–[15]. The minimum value $C_{jc\,\min}$ is reached, when the whole collector is depleted. For $J_c \to 0$, (4) approaches the common formula for depletion capacitances.

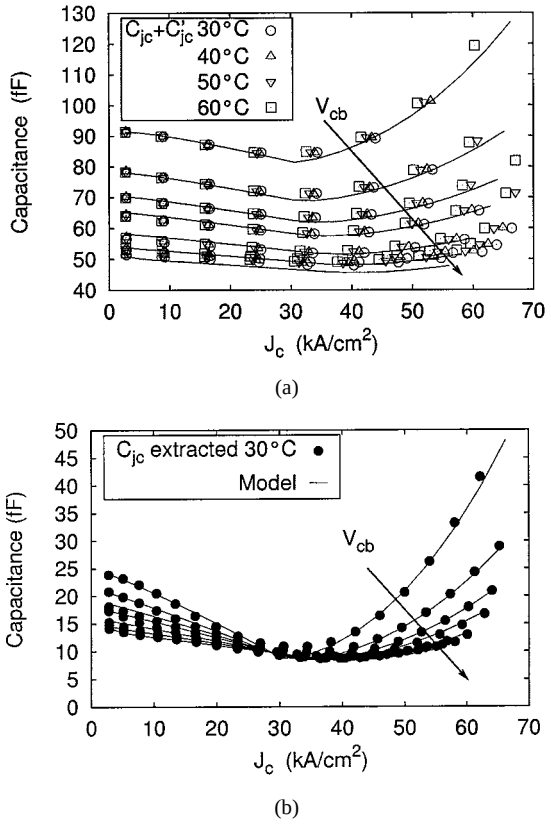

Fig. 2. Total base–collector capacitance $C_{\rm jc} + C'_{\rm jc}$ of $3 \times 15\ \mu{\rm m}^2$ HBT. (a) Extracted at different ambient temperatures. (b) Intrinsic base–collector capacitance $C_{\rm jc}$ with parameter $V_{\rm cb} = 0, 0.5, 1, 1.5, 2.5, 3.5, 4.5$ V (symbols: extracted values, lines: model).

In case of base push out, beyond $J_c \approx 30\,{\rm kA/cm}^2$, the capacitance increases. The empirical model formula for this region is

$$C_{\rm jc}\,|_{\rm high\ J_c} = C_{jc\,\rm min} + X_{Ck} \cdot C_{jc0} \cdot \left(\frac{J_c}{J_k} - 1\right)^{m'} \left(\frac{1}{1 - \dfrac{V_{\rm bc}}{\phi_{\rm bc}}}\right)^{n} \quad (5)$$

with $J_k = J'_{0a} - X'_{0a}/(V_{\rm cb} + V'_{0b})$, where J'_{0a}, X'_{0a}, V'_{0b}, X_{Ck}, and m' are fitting parameters. For the HBT shown here, $C_{\rm jc}$ increases according to a quadratic law with $m' = 2$.

The following two important conclusions can be drawn from the investigation of $C_{\rm jc}$:

- The effect of base push out is independent of temperature.
- The current density that determines the onset of the base push-out effect, i.e., J_k, increases with $V_{\rm cb}$.

On a first glance, this is in contradiction to the bias and temperature dependence of measured values of f_t. However, on the other hand, it agrees with analytical and numerical models that neglect temperature effects.

B. Transit Times

The small-signal extraction routine yields a time constant τ that is the sum of the emitter charging time τ_{BE}, base transit time τ_B, and collector transit time τ_C.

As a first step, the temperature dependence of τ is investigated. The junction temperature T_j is determined by

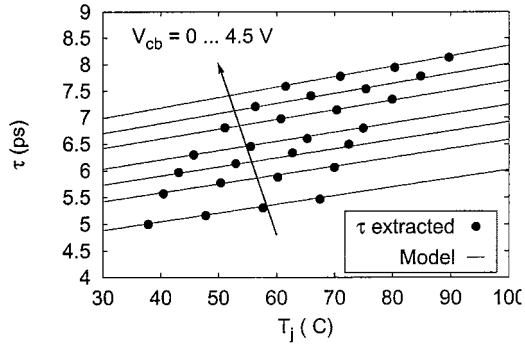

Fig. 3. Temperature dependence of τ at $J_c = 15$ kA/cm^2, $V_{\rm cb} \approx 0, \ldots, 4.5$ V, $T_{\rm amb} = 30, \ldots, 60$ °C.

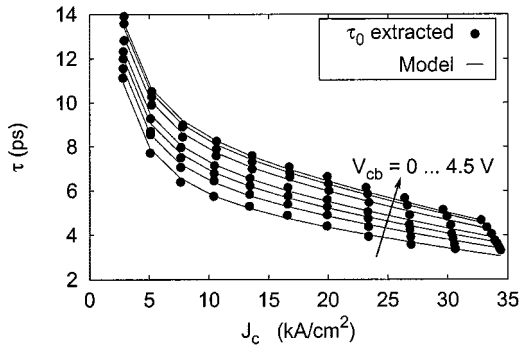

Fig. 4. Temperature-independent τ_0, extracted and modeled ($V_{\rm cb} \approx 0, \ldots, 4.5$ V, $T_{\rm amb} = 30$ °C).

$T_j = T_{\rm amb} + R_{\rm th} P_{\rm diss}$, with the ambient temperature $T_{\rm amb}$, the thermal resistance $R_{\rm th}$, and the dissipated power $P_{\rm diss}$. At a constant bias point, τ is found to depend linearly on temperature, as reported in the literature [16] (see Fig. 3). The bias dependence of the slope $\Delta\tau/\Delta T$ is found to be given mainly by two terms. The first is a constant, which is understood as the temperature dependence of the base transit time that also is assumed to be bias independent. The second contribution is proportional to $1/J_e$, similar to the emitter charging time τ_{BE}. The dependence of $\Delta\tau/\Delta T$ on base–collector voltage is very weak. It is considered in Fig. 3, but obviously can be neglected in the model.

Once the thermal behavior of τ is known, it can be separated from the bias dependence. In order to investigate the bias dependence, the transit time at constant junction temperature τ_0 is calculated (Fig. 4). It can be modeled by the following formula:

$$\tau_0 = \tau_{B0} + \frac{\kappa_{BE0}}{J_e} + \tau_C(V_{\rm bc},\, J_c) + \tau_{CIB}(V_{\rm bc},\, J_c). \quad (6)$$

The temperature-independent part of the base transit time τ_{B0} is assumed to be independent of bias. The emitter charging time $\tau_{BE0} = \kappa_{BE0}/J_e$ depends on emitter current density.

The third term in (6) is the collector transit time τ_C. It is a function of base–collector voltage and collector current density. In order to prove that the strong bias dependence of the total transit time τ in the range of moderate currents is caused by τ_C, it is helpful to consider the strong dependence of τ on collector doping. Fig. 5 shows a comparison of two HBTs with an emitter size of $3 \times 30\ \mu{\rm m}^2$. The only difference between these

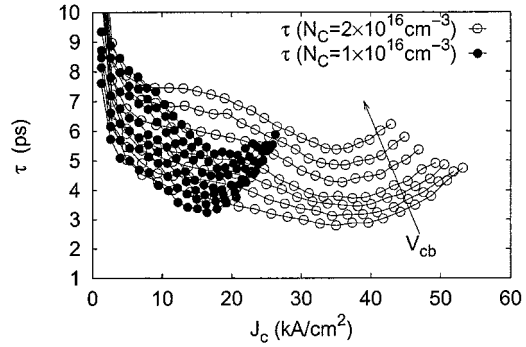

Fig. 5. Extracted values of τ for 3×30 μm^2 HBTs with ($\bullet$) $N_C = 1 \times 10^{16}$ cm^{-3} and ($\circ$) $N_C = 2 \times 10^{16}$ cm^{-3}, $V_{\rm cb} \approx 0, \ldots, 4.5$ V, $T_{\rm amb} = 30$ °C.

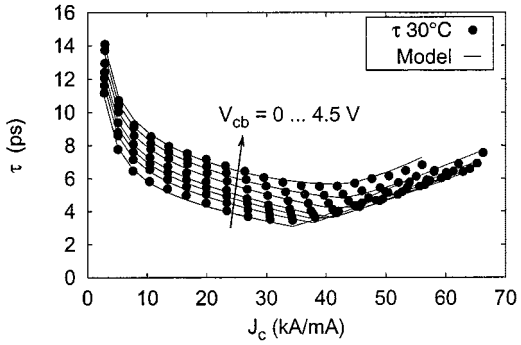

Fig. 6. Modeled and extracted total transit time τ, $V_{\rm cb} \approx 0, \ldots, 4.5$ V, $T_{\rm amb} = 30$ °C.

two HBTs is the collector doping, which is 1×10^{16} cm^{-3} for the first and 2×10^{16} cm^{-3} for the second transistor. Accordingly, the current that yields $N_{C,\rm eff} = 0$ ist twice as high for the second HBT. The behavior of τ is similar for both HBTs, only the J_c axis is stretched. It, therefore, can be concluded: 1) the bias-dependence of τ only is caused by the collector region (for J_c high enough that τ_{BE} can be neglected) and 2) that the respective parameters scale linearly with collector doping.

The collector transit time τ_C depends on current and voltage in a complex way. At low currents, τ_C increases with $V_{\rm cb}$ due to widening of the space–charge region. However, with increasing current and constant $V_{\rm bc}$, τ_C decreases, while the space–charge region increases due to lowered $N_{C,\rm eff}$. When the collector is fully depleted, τ_C increases with $V_{\rm cb}$. This behavior may be influenced by the negative slope of the field dependence of the electron velocity [5].

The dependence of τ_C on $V_{\rm bc}$ is modeled proportional to $1/C_{jcx} = 1/C_{\rm jc}|_{J_c \to 0}$ as follows:

$$\tau_C = (\kappa_{0i} - \kappa_{ui} J_c)/C_{jcx} + \kappa_{u0} J_c \tag{7}$$

with the fitting parameters κ_{0i}, κ_{ui}, and κ_{u0}. The linear dependence on J_c is, of course, not valid for all current densities. For lower currents, τ saturates in case of the HBT with higher collector doping in Fig. 5. This effect may be shadowed by the larger contribution of τ_{BE} for the other HBTs (Figs. 4 and 6). Also, it is assumed that τ_C approaches a constant value in the high-current range.

In the high-current regime, an additional transit time τ_{CIB} due to the current induced base region has to be considered. It is described by the following formula:

$$\tau_{CIB} = \frac{X_k}{Y_k + V_{\rm bc}^2} \cdot \frac{\left(\dfrac{J_c}{J_k} - 1\right)}{1 + X_\infty \left(\dfrac{J_c}{J_k} - 1\right)} \tag{8}$$

with $X_\infty = 2\pi f_\infty X_k/(Y_k + V_{\rm bc}^2)$. f_∞ denotes the minimum transit frequency, when the current-induced base region fills the whole collector, X_k and Y_k are parameters to describe the voltage-dependent slope of τ_{CIB}. No temperature dependence of this parameter is included since the main effect is the rapid degradation of f_t beyond the onset of the base push-out effect.

From this section, it can be concluded: 1) that the contribution of the bias-dependent collector transit time τ_C to the total transit time cannot be neglected and 2) the onset of base push out is better observed in $C_{\rm jc}$ since, in the transit times (and f_t), it is shadowed by temperature effects.

IV. Implementation into Large-Signal Model

The base–collector capacitance is modeled by a collector charge $Q_c = \int C_{\rm jc}(V_{\rm bc})\, dV_{\rm bc}$. The transcapacitance resulting from $dQ_c/dV_{\rm be} \neq 0$ is small up to the onset of base push out. The current I_k that determines the onset of base push out is approximated by a constant, in order to improve convergence of the harmonic-balance simulation. This is possible since the output current of a power amplifier reaches its maximum only within a narrow range of low voltages.

The transit times are usually described by the time constant of the base–emitter p-n junction, i.e., by C_{eD}, $C_{\rm je}$, and D_e. Therefore, the charge $Q_b = \int C_{eD}(V_{\rm be})\, dV_{\rm be}$ is modified in the new model.

The dependence of τ on $V_{\rm bc}$ is approximated by a linear function. Linear behavior is also reported in [17]. Its J_c dependence is described by a tanh characteristic. Additionally, to the parameter τ_{B0}, the bias dependence is modeled using the parameters τ_{C0}, τ_{cx}, τ_x, and $X_\infty = 2\pi f_\infty \tau_x$. τ_T describes the temperature dependence

$$\begin{aligned} Q_{b,\rm med}(v_{\rm bc}, I_c) &= (\tau_{B0} - \tau_{C0} \cdot v_{\rm bc}) \cdot I_c + \tau_{cx} \tanh\left(\frac{I_c}{I_k} - 1\right) \\ &\quad \cdot \left(1 - \frac{I_c}{I_k}\right) \end{aligned} \tag{9}$$

$$\begin{aligned} Q_{b,\rm high}(v_{\rm bc}, I_c) &= (\tau_{B0} - \tau_{C0} \cdot v_{\rm bc}) \cdot I_c \\ &\quad + \tau_x \left(\frac{\left(\dfrac{I_c}{I_k} - 1\right)}{1 + X_\infty \left(\dfrac{I_c}{I_k} - 1\right)}\right)^2 \end{aligned} \tag{10}$$

$$\begin{aligned} Q_{b,\rm new}(v_{\rm bc}, I_c, T_j) &= \begin{cases} \tau_T I_c \Delta T_j + Q_{b,\rm med}(v_{\rm bc}, I_c), & \text{for } I_c < I_k \\ \tau_T I_c \Delta T_j + Q_{b,\rm high}(v_{\rm bc}, I_c), & \text{for } I_c > I_k. \end{cases} \end{aligned} \tag{11}$$

V. Parameter Extraction

Input data are on-wafer microwave S-parameter and dc I–V measurements. The small-signal equivalent-circuit elements are determined at various bias points [6]. The parameters that are directly inserted into the large-signal model are the bias-independent extrinsic elements and the intrinsic base resistance R_{b2}, which turns out to be constant as well.

The parameters describing the base–collector junction capacitances $C_{\rm jc}$ and $C'_{\rm jc}$ are extracted from the bias dependence of the small-signal capacitances. S-parameter measurements in the off state yield the parameters describing the base–emitter junction capacitance $C_{\rm je}$. The diffusion capacitance C_{eD} and the base transit-time parameters are determined from the small-signal equivalent circuit.

The parameters describing the base–emitter diodes D_e, D'_e, and their temperature dependence are calculated from Gummel plots measured at different substrate temperatures. The thermal resistance is extracted from dc output characteristics, measured at two different temperatures, using an analytical procedure [18]. This measurement also yields the current gain β and its temperature dependence. The values of the base–collector diode D_c are estimated from the turn-on voltage in the output characteristics.

VI. Scaling of Model Parameters

In the following, the scaling of the equivalent-circuit parameters is discussed in detail.

Extrinsic Elements: As is easy to realize, these elements do not depend on dc bias and RF power and scale with the relevant areas of the device, e.g., the emitter area A_E. Detailed scaling rules are given in [10].

Base–Emitter Diodes: The saturation currents depend on the diode area. In case of the base–emitter diodes, this is the emitter area A_E. As shown in Fig. 1, there are two diodes in the base–emitter part of the device: The usual intrinsic junction diode D_e and the additional diode D'_e in series with R_x. The scaling of the temperature dependent parameters of (1) is given in Table I.

Base–Collector Diodes: These two diodes of the collector part represent the intrinsic junction diode D_c and the external diode D'_c. Their splitting ratio is $XC = 0.2$ for all sizes of transistors investigated. The current does not depend on temperature, the parameters are given in Table I. It should be noted that I_s is the very small saturation current of the usual diode characteristic (2), whereas the values $I_{s\infty}$ given for the base–emitter diodes are the maximum currents for $T \to \infty$, i.e., fictive quantities.

Depletion Capacitances: These capacitances scale in the same way as the diodes with the emitter area. The voltage dependence is given by $C(V) = C_0(1/(1 - V/\phi_d))^m$. The parameter X_{Ck} of $C_{\rm jc}$ from (5) is found to be 1.77. $C_{jc\,\rm min}$ is found to be 0.22 fF/μm^2. The other values are given in Table I.

Diffusion Capacitances, Transit Times, and Current Gain: The parameters for base and collector transit time $\tau_{B0} = 2$ ps, $\tau_{C0} = 240$ fs/V, $\tau_{cx} = 2$ ps, $\tau_T = 16$ fs/K, the excess transit-time factor $\tau_x = 13$ ps, the limitation factor $X_\infty = 0.08$, and the current gain $\beta = 100 \pm 5$ are independent of transistor geometry. The current gain decreases by 0.15/K with temperature.

TABLE I
Parameters of Diodes and Depletion Capacitances

Diode	$I_{s\infty}/A_E$	n	V_g	R_x/A_E
D_e	4 A/μm^2	1.01	1.58 V	—
D'_e	2 A/μm^2	1.4	1.37 V	360 $\frac{\rm M\Omega}{\mu\rm m^2}$
Diode	I_s/A_E			n
D_c	$XC \times 2.8 \times 10^{-20}$ A/μm^2			1.02
D'_c	$(1 - XC) \times 2.8 \times 10^{-20}$ A/μm^2			1.02
Cap.	C_0/A_E		m	ϕ_d
C_{jc}	$XC \times 2.28$ fF/μm^2		0.39	1.01 V
C'_{jc}	$(1 - XC) \times 2.28$ fF/μm^2		0.39	1.01 V
C_{je}	1.11 fF/μm^2		0.31	1.34 V

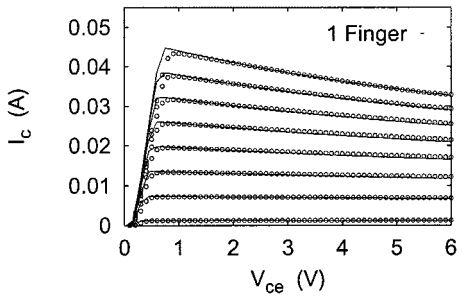

(a)

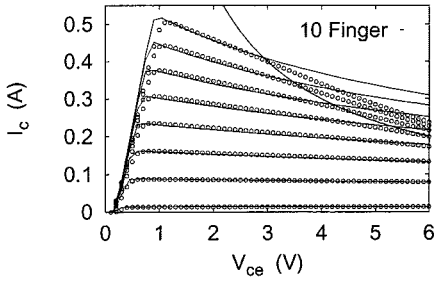

(b)

Fig. 7. DC characteristics of one- and ten-finger HBT. The model is valid up to 1.2-W dissipated power, indicated by the hyperbola (symbols: measurements, lines: simulation).

Onset of Kirk Effect: The current that determines the onset of the base push-out effect depends on emitter area $I_k/A_E = 3 \times 10^{-4}$ A/μm^2. I_0/A_E is chosen to be 4.5×10^{-4} A/μm^2.

Thermal Resistances: $R_{\rm th}$ depends on HBT periphery and layout and, due to mutual heating of the emitter fingers, no $1/A_E$ law applies. Therefore, a simple scaling rule with the number of emitter fingers cannot be derived. The values are $R_{\rm th} = 900$ K/W for the one-finger device, 430 K/W for the two-finger device, and 155 K/W for the ten-finger device.

VII. Results

In order to verify the above results, a set of model parameters was determined for the single-finger device and then scaled for two- and ten-finger devices using the scaling rules described above. DC characteristics of the one- and ten-finger HBT are compared in Fig. 7. The higher slope of the I–V characteristics

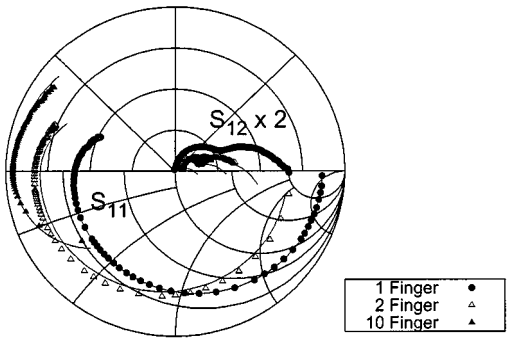

(a)

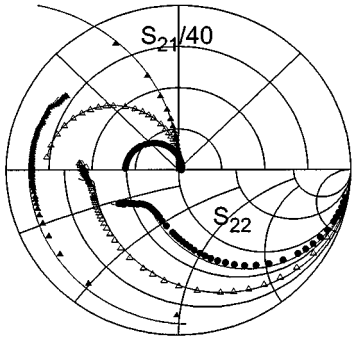

(b)

Fig. 8. (a) S_{11} and $S_{12} \times 2$ and (b) S_{22} and $S_{21}/40$ of a one-, two-, and ten-finger HBT at $V_{\rm cc} = 3$ V, $J_C = 40$ kA/cm^2, $f = 50$ MHz, ..., 50 GHz (symbols: measurements, lines: simulation).

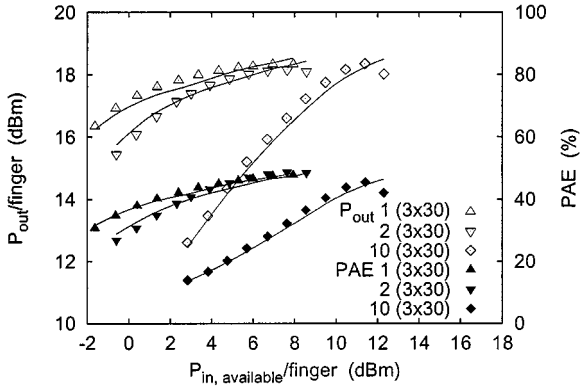

Fig. 9. Normalized output power and PAE versus normalized available input power at $J_C = 50$ kA/cm^2, 2 GHz for the HBTs with one, two, and ten fingers. The load is matched for maximum output power, second and third harmonics are terminated with 50 Ω (symbols: measurements, lines: simulation).

of the ten-finger HBT is caused by relatively higher $R_{\rm th}$ due to mutual heating of the emitter fingers. The model is accurate up to 1.2 W of dissipated power in case of the ten-finger HBT. Beyond this, a soft thermal breakdown occurs. Typical bias points are below this value. Measured and simulated S-parameters for the three types of HBTs are compared in Fig. 8. Generally, good agreement is found. Accuracy in the nonlinear case is demonstrated in Fig. 9. The results of harmonic-balance simulations using the model and load–pull measurements for all transistor sizes agree up to the saturation regime. The transistors exhibit

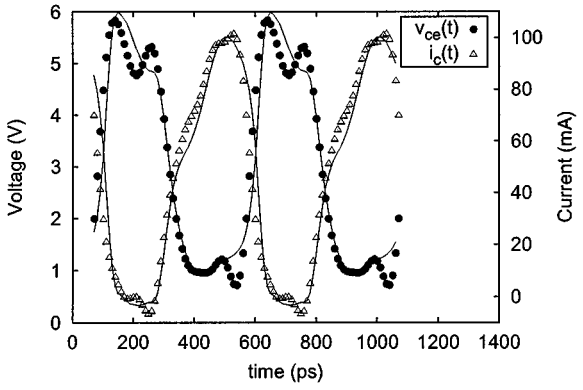

(a)

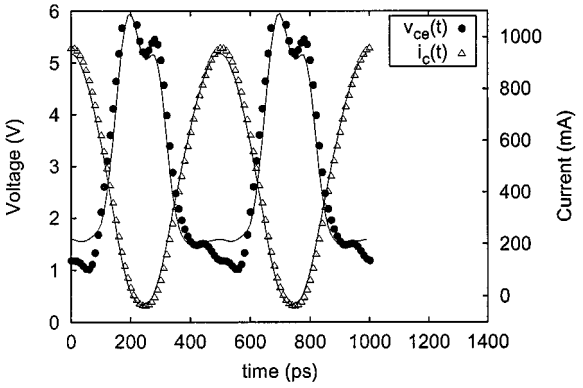

(b)

Fig. 10. Waveforms of collector–emitter voltage $v_{\rm ce}(t)$ and collector current $i_c(t)$ at 2 GHz. (a) $P_{{\rm in},\,av} = 6$ dBm (one-finger HBT) and (b) $P_{{\rm in},\,av} = 19.5$ dBm (ten-finger HBT) (symbols: measurements, lines: simulation).

18 dBm per emitter finger, while the power-added efficiency (PAE) decreases from 48% for the single-finger HBT to 46% in case of the ten-finger power cell.

Finally, Fig. 10 presents waveforms of collector current $i_c(t)$ and collector–emitter voltage $v_{\rm ce}(t)$. These measurements were taken under the same conditions as the previous measurements. The available source power $P_{\rm in,\,av}$ is 6 dBm for the single-finger HBT, 8 dBm for the two-finger HBT, and 19.5 dBm for the ten-finger HBT. While the amplitude of the voltages is given by the bias point $V_{\rm ce} = 3$ V, the currents scale with emitter size. The amplitudes of the currents are different since $P_{{\rm in},\,av}$ is only approximately scaled. The agreement between measurement and simulation is good for all sizes of HBTs.

VIII. Conclusions

A fully scalable HBT large-signal model for power applications has been presented in this paper. The model includes a new description for base–collector capacitance and transit times, in order to account for the bias-dependence of the base–collector space–charge region and the temperature dependence of the transit times. It is verified for one-, two-, and ten-finger HBTs operating at high-power levels up to 28-dBm output power for the ten-finger device. Only a single set of parameters is necessary for all cases. This simplifies parameter extraction, circuit design, and on-wafer device characterization.

ACKNOWLEDGMENT

The authors would like to thank the Material Technology and Process Technology Departments, Ferdinand–Braun–Institut für Höchstfrequenztechnik (FBH), Berlin, Germany, for providing the HBTs, S. Schulz, FBH, Berlin, Germany, and T. Spitzbart, formerly with FBH, Berlin, Germany, for performing measurements, and Dr. W. Heinrich, FBH, Berlin, Germany, and Prof. H. L. Hartnagel, Technische Universität Darmstadt, Darmstadt, Germany, for helpful discussions and continuous encouragement.

REFERENCES

[1] C. T. Kirk, Jr., "A theory of transistor cutoff frequency (f_t) falloff at high current densities," *IRE Trans. Electron Devices*, vol. ED-12, pp. 164–174, Mar. 1962.

[2] R. J. Whittier and D. A. Tremere, "Current gain and cutoff frequency falloff at high currents," *IEEE Trans. Electron Devices*, vol. ED-16, pp. 39–57, Jan. 1969.

[3] W. Liu and J. S. Harris, "Current dependence of base–collector capacitance of bipolar transistors," *Solid-State Electron.*, vol. 35, no. 8, pp. 1051–1057, Aug. 1992.

[4] R. G. Davis and M. B. Allenson, "Unified HBT base push-out and base–collector capacitance model," *Solid-State Electron.*, vol. 38, no. 2, pp. 481–485, Feb. 1995.

[5] L. H. Camnitz, S. Kofol, T. Low, and S. R. Bahl, "An accurate, large signal, high frequency model for GaAs HBTs," in *GaAs IC Symp. Dig.*, 1996, pp. 303–306.

[6] M. Rudolph, R. Doerner, and P. Heymann, "Direct extraction of HBT equivalent circuit elements," *IEEE Trans. Microwave Theory Tech.*, vol. 47, pp. 82–84, Jan. 1999.

[7] C. M. Snowden, "Large-signal microwave characterization of AlGaAs/GaAs HBT's based on a physics-based electrothermal model," *IEEE Trans. Microwave Theory Tech.*, vol. 45, pp. 58–71, Jan. 1997.

[8] T. Peyretaillade, M. Perez, S. Mons, R. Sommet, P. Auxemery, J. C. Lalaurie, and R. Quéré, "A pulsed-measurement based electrothermal model of HBT with thermal stability prediction capabilities," in *IEEE MTT-S Int. Microwave Symp. Dig.*, 1997, pp. 1515–1518.

[9] R. Hajji and F. M. Ghannouchi, "Small-signal distributed model for GaAs HBT's and S-parameter prediction at millimeter-wave frequencies," *IEEE Trans. Electron Devices*, vol. ED-44, pp. 723–732, May 1997.

[10] M. Rudolph, R. Doerner, E. Richter, and P. Heymann, "Scaling of GaInP/GaAs HBT equivalent-circuit elements," in *GAAS'99 Dig.*, pp. 113–116.

[11] M. Achouche, T. Spitzbart, P. Kurpas, F. Brunner, J. Würfl, and G. Tränkle, "High performance InGaP/GaAs HBT's for mobile communications," *Electron. Lett.*, vol. 36, no. 12, pp. 1073–1075, June 2000.

[12] P. C. Grossman and J. Choma, Jr., "Large signal modeling of HBT's including self-heating and transit time effects," *IEEE Trans. Microwave Theory Tech.*, vol. 40, pp. 449–464, Mar. 1992.

[13] C.-J. Wei, J. C. M. Hwang, W.-J. Ho, and J. A. Higgins, "Large-signal modeling of self-heating, collector transit-time, and RF-breakdown effects in power HBT's," *IEEE Trans. Microwave Theory Tech.*, vol. 44, pp. 2641–2647, Dec. 1996.

[14] Q. M. Zhang, H. Hu, J. Sitch, R. K. Surridge, and J. M. Xu, "A new large signal HBT model," *IEEE Trans. Microwave Theory Tech.*, vol. 44, pp. 2001–2009, Nov. 1996.

[15] A. Samelis, "Modeling the bias dependence of the base–collector capacitance of power heterojunction bipolar transistors," *IEEE Trans. Microwave Theory Tech.*, vol. 47, pp. 642–645, May 1999.

[16] D. A. Ahmari, G. Raghavan, Q. J. Hartmann, M. L. Hattendorf, M. Feng, and G. E. Stillman, "Temperature dependence of InGaP/GaAs heterojunction bipolar transistor DC and small-signal behavior," *IEEE Trans. Electron Devices*, vol. 46, pp. 634–640, Apr. 1999.

[17] B. A. Kramer and R. J. Weber, "Base–emitter diffusion capacitance in GaAlAs/GaAs HBTs," *Electron. Lett.*, vol. 28, no. 12, pp. 1106–1107, June 1992.

[18] N. Bovolon, P. Baureis, J.-E. Müller, P. Zwicknagl, R. Schultheis, and E. Zanoni, "A simple method for the thermal resistance measurement of AlGaAs/GaAs heterojunction bipolar transistors," *IEEE Trans. Electron Devices*, vol. 45, no. 8, pp. 1846–1848, Aug. 1998.

Matthias Rudolph (M'99) was born in Stuttgart, Germany, in 1969. He received the Dipl.-Ing. degree in electrical engineering from the Technische Universität Berlin, Berlin, Germany, in 1996, and is currently working toward the Dr.-Ing. degree at the Ferdinand–Braun–Institut für Höchstfrequenztechnik, Berlin, Germany.

His research focuses on characterization and modeling of FETs and HBTs.

Ralf Doerner (M'97) was born in Neindorf, Germany, in 1965. He received the Dipl.-Ing. degree in communications engineering from the Technische Universität Ilmenau, Ilmenau, Germany, in 1990.

Since 1989, he has been involved with microwave measuring techniques. In 1992, he joined the Ferdinand–Braun–Institut für Höchstfrequenztechnik, Berlin, Germany. His current research is focused on calibration problems in on-wafer millimeter-wave measurements of active and passive devices and circuits and on nonlinear characterization of microwave power transistors.

Klaus Beilenhoff (M'90) received the Dipl.-Ing. degree in electrical engineering and the Dr. Ing. degree from the Technical University of Darmstadt, Darmstadt, Germany, in 1989 and 1995, respectively.

During his post-graduate studies he was involved with the field-theoretical analysis and modeling of coplanar waveguide (CPW) discontinuities using the finite-difference method in frequency domain. From 1995 until the beginning of 2000, he was a Research Assistant at the Institut für Hochfrequenztechnik, Technical University of Darmstadt, Darmstadt, Germany, where he was engaged in the design and field-theoretical analysis of MMICs. Since February 2000, he has been with Daimler Chrysler AG, Stuttgart, Germany, where he is engaged in the area of technology transfer. In particular, he is working together with United Monolithic Semiconductors in Orsay, France and Ulm, Germany.

Peter Heymann (A'95) was born in Berlin, Germany, in 1939. He received the Dipl.-Phys. and Dr. rer.-nat. degrees in physics from the University of Greifswald, Greifswald, Germany, in 1963 and 1968, respectively.

From 1963 to 1982, he was involved with different projects in the field of wave–plasma interaction, which include wave propagation, RF plasma sources and heating, and microwave and far-infrared plasma diagnostics. Since 1982, he has been involved with GaAs microwave electronics. In 1992, he joined the Ferdinand–Braun–Institut für Höchstfrequenztechnik, Berlin, Germany, where he is currently responsible for measurements, characterization, and modeling of active and passive components of microwave MMICs.